

Resonance Fluorescence Spectroscopy of a single quantum dot with the attoCFM I

Elena Kammann¹, Sebastian H. E. Müller¹, Katja Puschkarsky², Matthias Hauck², Sarah Beavan², Alexander Högele², and Khaled Karraï¹

¹attocube systems AG, Munich, Germany

²Ludwig Maximilian Universität, Munich, Germany

I. Introduction

Resonance fluorescence spectroscopy of semiconductor quantum dots (QDs) [1, 2, 3, 4, 5] and other single photon emitters, such as vacancy centers [6] often yields more information about the emitters than the more commonly used non-resonant excitation. However it is a technically challenging measurement to perform. The difficulty lies within the separation of the excitation laser photons from the re-emitted and scattered photons. One way in which this can be achieved is by means of polarization suppression: in a geometry where the scattered laser photons have a well-defined polarization, they can be filtered from the detected signal facilitating the detection of resonance fluorescence (RF). The confocal microscope presented in section II is designed to combine a high polarization extinction ratio (ER) for efficient RF measurements with low temperature and high magnetic field compatibility. In par-

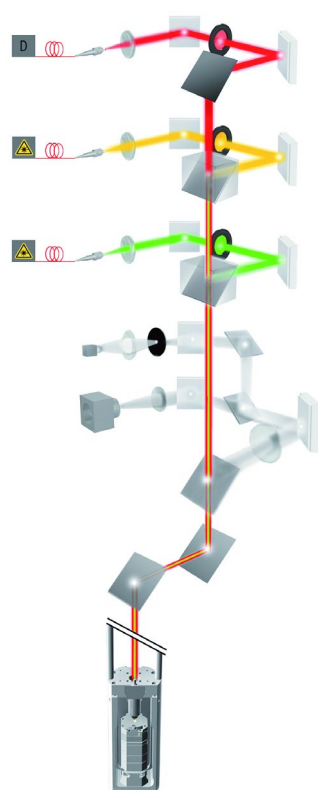


Figure 1: 3D-Scheme of the attoCFM I consisting of two excitation channels (green and yellow) and one detection channel (red), the inspection optics (light grey), for wide field imaging of the sample. The housing comprised of the objective and the 3D positioning system, which carries the sample, is located in the cryogenic space.

particular we present the first low temperature microscope with apochromatic performance in the near infrared spectral range. Such a setup allows for convenient switching between resonant and non-resonant excitation without the need for re-alignment, as shown in II.3.

In order to demonstrate the functionality of the instrument in high spatial and spectral resolution spectroscopy, we performed measurements on single gate-voltage controlled QDs, such as described in section III. Section IV describes the first observation of RF, as well as the associated Mollow triplet [7], obtained with a commercially available system.

II. The cryogenic confocal optical microscope

In this section, the measurement setup and its basic characteristics are described. The cryo-compatible microscope head is outlined in sub-section II.1 and subsequently the excitation lasers and the detectors used for the experiments are presented in II.2 and II.3 respectively. The characteristics of the low temperature apochromatic objectives are discussed in subsection II.4 and details on the polarization suppression can be found in subsection II.5.

II.1. The optical microscope

The optical setup is based on the attoCFM I, attocube's commercial confocal microscope designed specifically for applications at low temperature and high magnetic field. The microscope head, shown in Figures 1 and 2 includes several

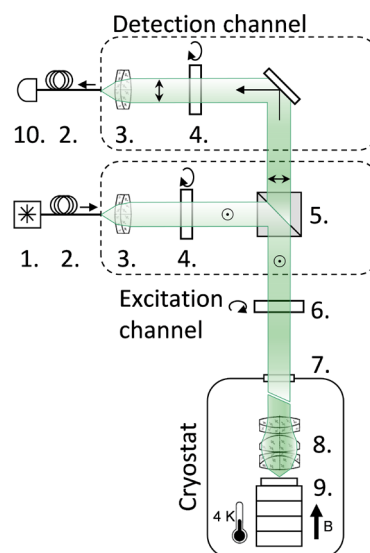


Figure 2: Schematic of the polarization suppression option. An excitation laser (1.) is coupled into the microscope by a single mode fiber (2.) and a collimation lens (3.). The polarization is defined by a nanoparticle plate polarizer on a rotator (4.) such that the excitation light is reflected by the polarizing beam splitter cube (5.). A quarter-wave plate (6.) allows for switching between suppression and transmission mode. The cold space is separated by an optical window (7.) and the light is focused by an apochromatic low temperature objective (8.) onto a sample mounted on a piezo positioning stack (9.). The p-polarized fraction of the collected light passes to the detection channel and is recorded with a photodetector (10.).

excitation and detection channels, as well as an inspection unit allowing for wide field imaging of the sample. We took particular care during the design of the microscope head to achieve high mechanical rigidity of the structure, resulting in unprecedented stability against drift [8]. Furthermore, the excitation and collection paths can be aligned separately, which facilitates a straight-forward and systematic alignment procedure. The head is mounted onto a microscope stick which is inserted in a thin wall stainless steel vacuum tube. This vacuum tube, filled with low pressure, pure helium exchange gas, in turn is cooled in a top loading ultra-low vibration closed cycle cryostat (attoDRY1000) to temperatures in the lower Kelvin range. Alternatively, the microscope and its insert can be plunged in a bath of liquid helium in a standard dewar.

The objective and the sample position handling are rigidly mounted in a common compact housing of 49 mm in diameter and placed at the bottom of the microscope stick. The compact microscope head experiences a homogeneous temperature at all times, preventing drifts due to temperature gradients. The excitation light is collimated in the head assembly, enters through a vacuum sealed window on the top of the stick and propagates freely to the objective's back aperture. The re-emitted or scattered light traces back the same pathway back to the detection unit. The sample is held by a piezo-positioner stack, allowing for precise positioning and focusing at cryogenic temperatures.

II.2. Laser excitation sources

A single mode laser diode, tunable from 920 - 980 nm (Sacher Lion Metcalf Laser System TEC500) is used for resonant spectroscopy. For the non-resonant excitation a laser diode at 850 nm (Roithner Lasertechnik GmbH, LJ-series) is used. Both lasers are coupled into single mode fibers and launched into the fiber ports of the microscope. In order to retain the collimation, excitation and collection, fibers are permanently attached to the microscope head and the different lasers were coupled by using fiber connectors.

II.2. Detection system

The emission is collected through a single mode fiber and detected with a spectrometer or an avalanche photo diode (APD, <100 dark counts by Excelitas) connected to a gated photon counter. A home-made Fabry-Pérot tunable filter is used in order to spectrally resolve the emission with a resolution of 100 MHz. Beneath the sample the transmitted intensity is recorded on a photodiode. The gate voltage applied on the sample was modulated around the average voltage value at 77 Hz with a square wave form. The signal demodulated by a lock-in amplifier yielded the differential transmission of the quantum dot [9]. The average gate voltage value was swept continuously. This in turn tunes the QD optical transition through the resonance with the excitation laser by means of the quantum confined Stark Effect.

II.3. The apochromatic objective

The mapping, localization and characterization of an appropriate single quantum emitter prior to the resonant experiment were performed under non-resonant excitation. In this context, the use of a standard aspheric lens is problematic [10] because of chromatic aberrations that yields different focal planes for the non-resonant excitation laser and the resonant laser/emission. While achromatic performance is generally assumed as given in confocal microscopy at room temperature, this is not trivial for cryogenically cooled microscopes. To eliminate this problem, low temperature-compatible objectives with an apochromatic range in the near infrared (700 - 1010 nm) were designed. The apochromatic range is defined as the range of wavelengths that focus within the depth of focus, given by $n\lambda_{ref}/NA^2$, where λ_{ref} is chosen to maximize the apochromatic range and n is the index of refraction. This range is relevant for a number of applications, including cryogenic spectroscopy of III-V alloy QDs.

Figure 3 shows the calculated focal shift as a function of wavelength for the three apochromatic objectives currently available from attocube systems. The focal shift of an aspheric lens typically used in RF experiments [2] is also shown for comparison. In our experiments the QDs emit at around 960 nm and the non-resonant excitation is performed at 850 nm. The chromatic focal shift between those two wavelengths of the aspheric lens amounts to 8 μm , whilst the shift for the LT-APO/IR/0.75 remains below the depth of focus of 1.7 μm , which demonstrates the superiority of the apochromatic objectives.

The effective focal length of the LT-APO/IR/0.75 is 3.13 mm, the working distance of 0.65 mm is compatible with the use of solid immersion lenses, and the clear aperture of 4.7 mm is adapted to the collimation optics.

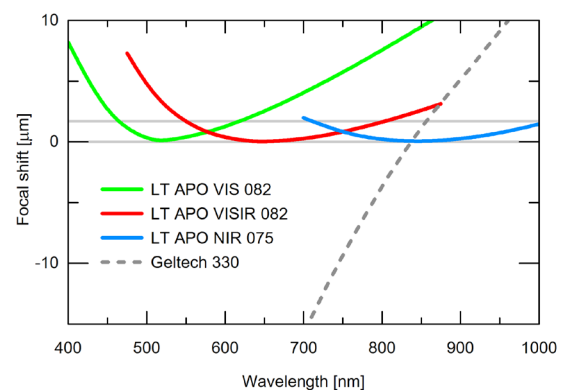


Figure 3: Calculated focal plane shift as a function of wavelength for the 3 apochromatic objectives available at attocube systems. The Geltech 330 is often used in RF measurements [2] but shows extremely poor achromatic behavior making it very difficult to use for combined luminescence and resonant spectroscopy. For the LT-APO/IR/075 the calculated focal displacement remains within the diffraction limited depth of focus of 1.7 μm indicated by the grey line for the LT-APO/NIR/075 (for $\lambda_{ref} = 955 \text{ nm}$).

Temperature [K]	Wavelength [nm]	Transmission Spotsizesize [μm]	Reflection Resolution [μm]
300	850	1.25 ± 0.08	1.01 ± 0.09
4	850	1.18 ± 0.07	0.96 ± 0.10
300	960	1.21 ± 0.06	1.11 ± 0.11
4	960	1.21 ± 0.09	1.03 ± 0.07

Table 1: Summary of the spotsizesize measurements at 4 K and room temperature. The values correspond to the full width at half maximum (FWHM).

A crucial parameter for the performance of the microscope is the quality of the spot formed by the objective, as it determines the resolution of the system, as well as the excitation density and the collection efficiency that can be achieved. We measured the size of the spot by sweeping it across a calibrated grating while tracking the transmitted as well as the reflected light intensity.

The measurement in transmission yields the size of the focal spot, whilst the reflected signal gives the actual resolution of the whole system. The 960 nm laser was coupled via a 2x2 fiber beam-splitter to the excitation (detection) channel of the microscope, such that the back reflected signal from the grating surface could be measured. The grating was moved into the focal plane by maximizing the reflected intensity collected back into the excitation (detection) channel. The focal position is adjusted for 960 nm at room temperature. Next, the 850 nm laser is connected to the microscope fiber and the measured spot-size is found to be constant within the error bars. The experiment was repeated at 4 K. The results of all measurements are summarized in Table 1. Note that the measurements demonstrate the achromaticity of the entire system, including the collimation optics.

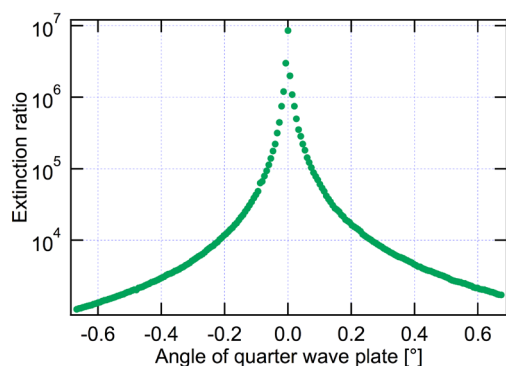


Figure 4: The extinction ratio plotted as a function of the angle of the quarter wave plate. In a narrow angular region of about 30 m° the extinction exceeds six orders of magnitude ultimately demonstrating the need for high resolution piezo-driven rotators.

II.4. Polarization suppression

The key parameter of a polarization darkfield microscope is the extinction ratio, namely $ER = I_{max}/I_{min}$, where I_{max} corresponds to the intensity of photons reflected from the sample and detected in a collinear configuration of the polarizer and the analyzer, and I_{min} is obtained in a cross-polarized configuration. In an ideal system I_{min} is zero and the ER diverges, but in reality it corresponds to the imperfection of the cross-polarization scheme and is called the leakage signal. For an RF measurement on a single semiconductor QD the extinction ratio ER should exceed 10^5 in order to detect a reasonable ratio of the weak QD signal relative to the shot-noise inherent to the laser leakage background.

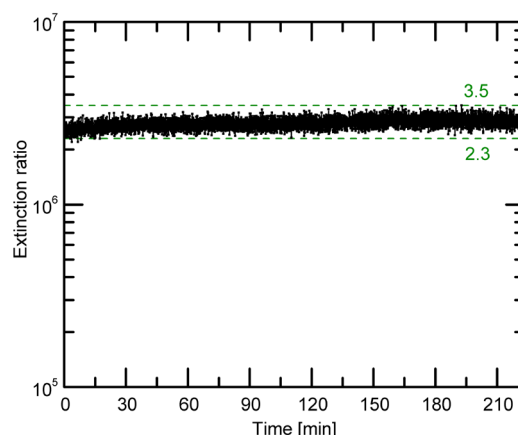


Figure 5: The extinction ratio tracked over a period of 3.5 hours.

In the confocal microscope the polarization optics are integrated according to the scheme in Figure 2. A polarizing beam splitter cube is placed into the lower unit (excitation unit), which reflects the s-polarized light towards the sample. The laser reflected back from the sample is directed back into the excitation channel such that only residual laser light enters the collection optics. The back-scattered laser light in this configuration is suppressed by about 3 orders of magnitude. In order to increase the extinction, plate polarizers are inserted into the excitation and the detection channels where they support the action of the cube polarizer (4. in Figure 2). Precision attocube stepping piezo rotators (ECR4040AP) are crucial for the sensitive alignment of the polarizers along the axes of the polarizing cube [2]. The configuration of the microscope can be switched from maximum extinction to maximum transmission by rotating a quarter-wave plate beneath the microscope on a second attocube rotator. The quarter-wave plate also reverses ellipticities that are unintentionally induced along the beam path in the microscope, which requires ultra-precise alignment facilitated by ECR4040AP rotator. The system is aligned in the maximum transmission configuration and the ratio of the minimum and maximum values measured in the two configurations correspond to the extinction ratio.

For maximization of the ER the rotators carrying the polarizers and the waveplate are rotated until the ratio between I_{max} and I_{min} is maximized. In Figure 3 the evolution of the extinction ratio as a function of the orientation of the wave-plate is shown. It is observed that for a very small angular range within 30 m° only, the extinction ratio is adjusted to exceed 10^6 rendering piezo-driven rotators, such as the ECR4040AP, essential for reaching extreme extinctions.

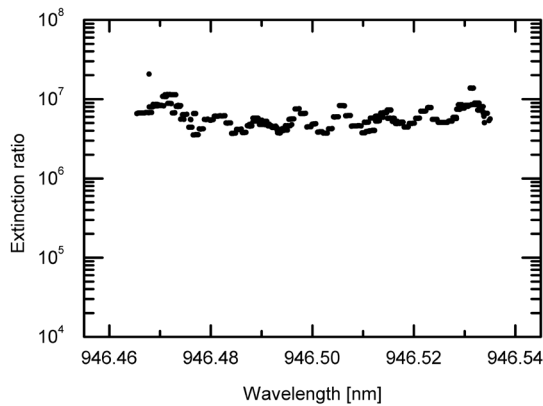


Figure 6: The extinction ratio during a wavelength-sweep of $\sim 70\text{ pm}$.

Further, we observed that these extremely high extinctions ratio can only be reached when the tunable narrow band external cavity laser diode is used (Sacher Metcalf). In a comparison experiment using a standard laser diode (Roithner Lasertechnik GmbH, 960 nm) a dependency of the extinction on the quality of the laser is observed. Using the narrowband source an extinction of 3×10^7 was reached, whilst using the diode laser the extinction was limited to 1.8×10^6 , with the exact same optical alignment. Using a 905 nm laser diode, the extinction is limited to the 10^5 range. This observation can be attributed to the excess non lasing background photons in diode lasers used without internal spectral filtering, such as the latter two laser diodes. In general it is found that the extinction ratio that can be achieved varies between 10^6 and 10^8 , when the tunable diode laser is employed.

In order to carry out long and demanding experiments on single photon emitters the stability of the ER over time is of utmost importance. The stability of the extinction is demonstrated by tracking the counts on the APD over more than 3 hours. The ER during this period remains strictly above 10^6 (see Fig. 5).

Finally we show that the setup can also be used for single quantum emitters without a gate-tunable resonance, where instead of the gate voltage the wavelength can be swept across the resonance. In Figure 6 the ER is shown as a function of wavelength for a narrow band wavelength-sweep of $\sim 70\text{ pm}$. For comparison the linewidth of a QD resonance is of the order of 5 pm. We observe that for this range the ER remains well above 10^6 .

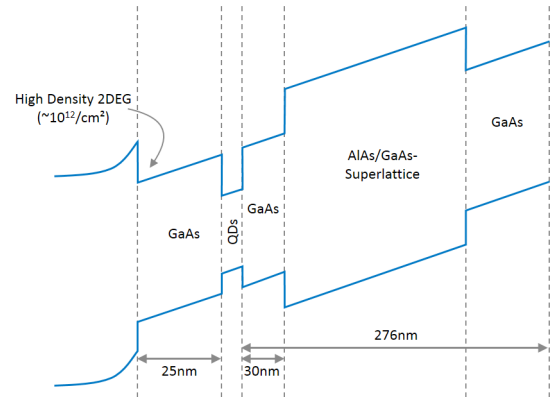


Figure 7: Band-structure schematic of the sample.

III. The sample

The sample under investigation contains self-assembled InGaAs QDs grown by molecular beam epitaxy [11] embedded inside a field effect device [12] (see Fig. 7) grown at UC Santa Barbara in the group of P. M. Petroff. The QD heterostructure can be controlled by a semitransparent top electrode formed by a thin semi-transparent layer of NiCr, which is evaporated on the surface of the sample. The gate voltage which can be applied to the top electrode shifts the QD resonances with respect to the Fermi level. This allows for charge carriers to be loaded one by one into the QD [13]. Furthermore the exciton emission energy can be tuned by means of the quantum confined Stark effect [14].

IV. Resonance fluorescence measurements

In this section the measurement strategy to obtain RF data with a gate tunable QD sample is outlined and the results from the different steps are discussed.

In the first step an appropriate QD for the RF investigation is selected by mapping the photoluminescence spectrum as a function of the gate voltage. The sample is excited off-resonantly by the 850 nm laser diode and the emis-

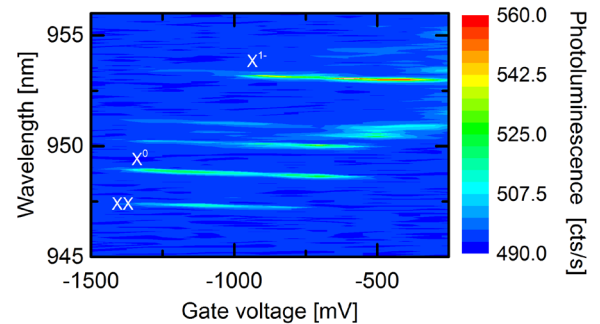


Figure 8: The photoluminescence spectra as a function of the gate voltage. Here, three different charge states of the quantum dot is revealed through its various exciton emission lines (Neutral exciton X^0 , negatively charge exciton X^- , and biexciton XX)

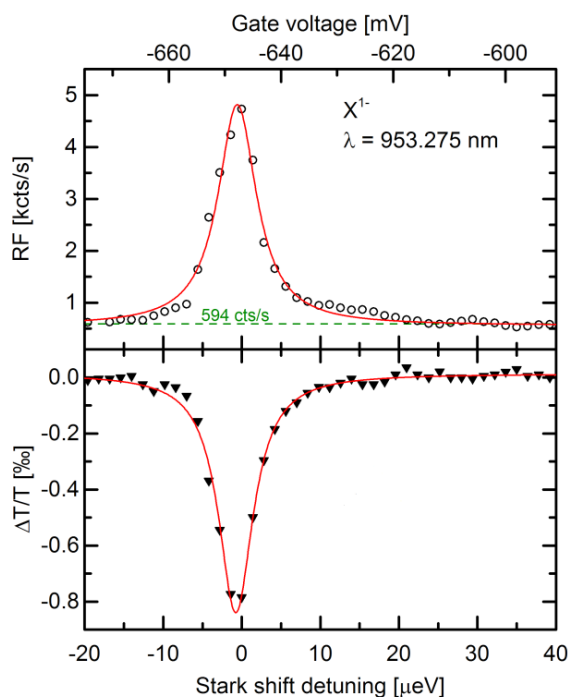


Figure 9: Simultaneously taken RF (empty circles in the upper panel) and differential transmission spectra (filled triangles in the lower panel) with the corresponding Lorentzian fits. The extinction ratio amounts to 10^6 .

sion is directed to the grating spectrometer. At this stage the microscope should already be roughly adjusted to the suppression mode, such that the laser does not enter the collection fiber and the fluorescence thereof is minimized. The QD modes are easily identifiable in a PL-map (Fig. 8), according to reference 13.

For the RF experiments we chose to investigate the negatively charged exciton X^{1-} as the transition is unpolarized at zero magnetic field [15]. Consequently the resonant fluorescence has significant emission with a polarization orthogonal to the excitation laser. Furthermore the X^{1-} emission is not expected to depend on the crystallographic orientation of the QD, as it would for an X^0 .

Next the gate voltage is tuned to favor X^{1-} stable photoluminescence and the resonant laser is adjusted on the spectrometer to the X^{1-} emission wavelength. The ER can now be conveniently maximized by minimizing the laser background counts on the spectrometer. At this point the microscope is adjusted to the suppression mode and ready for the RF measurements.

Simultaneously with the RF differential transmission is also acquired [9] for the sake of direct comparison. To this end the gate voltage is modulated with amplitude of 200 mV whilst scanned and the differential transmission is recorded by means of the transmission photodiode and demodulated, using a lock-in amplifier. At the same time the fluorescence photons, which are collected through the collection path of the microscope are recorded on the avalanche photodiode. Taking both measurements simultaneously allows for a direct comparison between the two

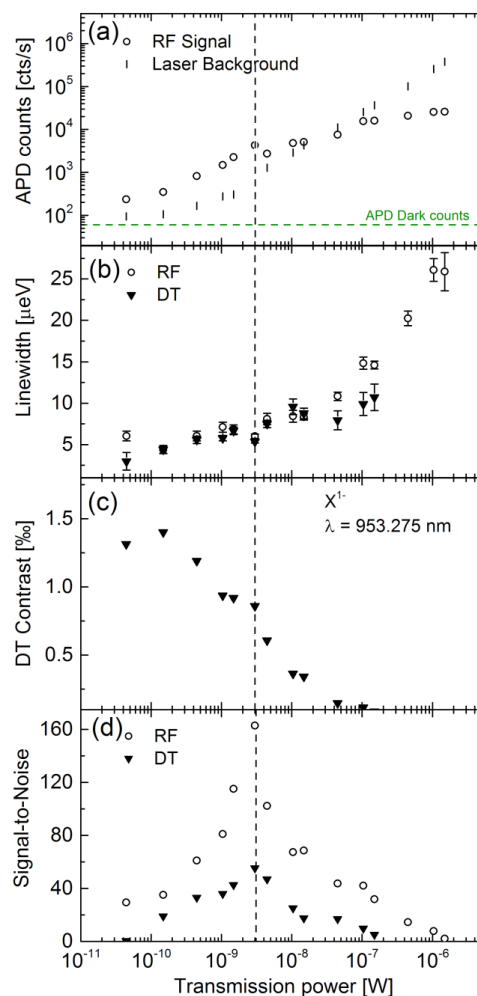


Figure 10: Power dependence of a single quantum dot resonant transmission and resonance fluorescence. (a) The RF counts (circles) and the background counts from the laser (vertical lines). (b) Line-widths at half maximum extracted from a Lorentzian fit to the data. (c) Signal contrast of the resonant transmission measurements. (d) Signal to noise ratio of RF and transmission measurements. The vertical line marks the power where the best signal to noise ratio is obtained.

techniques. Figure 8 displays the simultaneously taken differential transmission and RF spectra.

Both the resonant transmission and fluorescence were measured and analyzed over a broad range of powers. The detection counts of the resonant emission signal are displayed in Figure 10 (a). A clear saturation of the fluorescence counts can be observed. The linewidth (Fig. 10 (b)) increases monotonically due to power broadening, which can be monitored in both resonant measurements. A larger range of powers is accessible to the RF, as the differential transmission contrast fades in the noise level at high laser powers (Fig. 10 (c)). The largest signal to noise ratio (Fig. 10 (d)) in transmission and in fluorescence is marked by the vertical dotted line and it coincides with the inflection point of the differential transmission contrast. We find that the signal to noise ratio is about three times higher in RF measurements, as it is in transmission, making the RF a powerful high resolution spectroscopy technique.

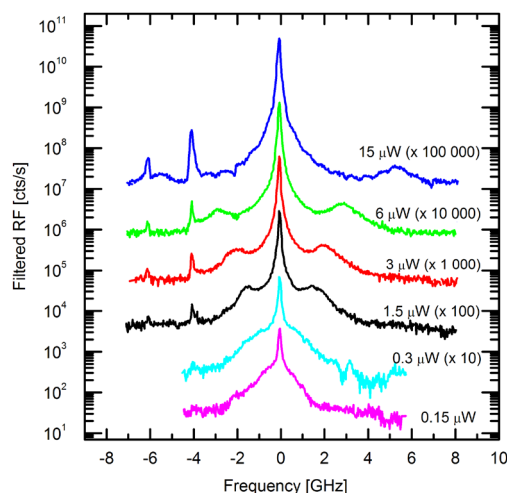


Figure 11: The resonant quantum dot emission filtered through a high finesse scanning Fabry-Pérot spectral filter reveals a central and two side peaks (Mollow triplet), which move away from the central resonance with increasing excitation power. (The sharp peaks at -4 and -6 GHz correspond to the laser leaking through higher order Fabry-Pérot modes).

It should be pointed out that the impressive high light emission rates of several hundred thousands of counts per second that has been achieved in ref. 2, was not observed in the present measurements due to the sample quality. First, the low power linewidth limit amounts to $\sim 6 \mu\text{eV}$ being much broader than the usual 1 to 2 μeV measured on better QDs [2]. We noticed that the low fluorescence yield of the sample is already present in PL measurements where the counts saturate at ~ 1000 cts. This number is far from the estimated counts according to the cycling rate corresponding to a lifetime of ~ 1 ns ($\sim 100\,000$ cts/s after correction for collection and detector efficiencies), which is typical for gate-tunable InGaAs QDs [16]. The low count rates are consistent with previously obtained results taken with a microscope constructed according to the descriptions in ref. 2. The collection efficiency, and therefore the RF counts, could further be improved by using a solid immersion lens, which is expected to increase the number of counts by a factor of four to five [17]. In any case choosing to test our setup on poorly emitting QDs is the perfect “stress-test” for our instrument showing that it can be easily used on poorer single quantum emitters.

Finally, the resonant measurements just shown previously are obtained by sweeping the exciton emission wavelength in resonance with the probing laser wavelength. In the next step, the gate voltage is fixed such that the laser directly coincides with the maximum of the RF. The emission is filtered through a Fabry-Perot spectral filter. This allows for the resolution of the side bands at high excitation power, referred to as the Mollow triplet [7], which is shown in Figure 10. This triplet is a pure quantum optical signature of the hybridization of the photon-exciton fields. It has previously been observed in QDs [19] and was interpreted as a characteristic feature of a quantum optical solid-state two-level system in close analogy to atoms [18] or molecules [19].

V. Summary

In summary we presented a setup for low temperature high resolution laser spectroscopy. The unique feature of this setup is the apochromatic performance that permits alignment free switching between off-resonant PL measurements and RF. This feature is fully enabled by our novel cryogenic compatible apochromatic objectives designed to hold the focus plane at the same position on the sample independently from the photon wavelength.

The commercially available polarization extinction option of the attoCFM I confocal head combines for the first time the use of high precision rotators within the flexible beam-management. This enabled us to achieve extinction ratios of 10^7 , a factor just 10 away from world record in research labs [2] while allowing an unprecedented flexibility of use. We conducted the first RF measurements on a single quantum emitter obtained with a commercial system and demonstrated the simultaneity of the measurement with resonant transmission laser spectroscopy confirming the full correlation between the two forms of measurements. The RF is found to have a signal to noise advantage of 300%. High resolution spectroscopy reveals the splitting of the QD mode at high excitation powers, known as the Mollow-Triplet.

Finally, we would like to stress that the application of our instrument is not limited to the study of gate-controlled quantum dots, but can also be employed for quantum dots or other single photon emitters with a fixed resonance, by scanning the resonant laser excitation at constant extinction.

References

- [1] A. N. Vamivakas *et al.*, *Nature Physics* **5**, 198 (2009).
- [2] A. V. Kuhlmann *et al.*, *Review of Scientific Instruments* **84**, 073905 (2013).
- [3] A. V. Kuhlmann *et al.*, *Nature Physics* **9**, 570 (2013).
- [4] A. Ulhaq *et al.*, *Nature Photonics* **6**, 238 (2012).
- [5] M. Munch *et al.*, *Nature Nanotechnology* **9**, 671 (2014).
- [6] T. Müller *et al.*, *Nature Communications* **5**, 3328 (2014).
- [7] B. R. Mollow, *Physical Review* **188** (1969).
- [8] <http://attocube.com/attomicroscopy/high-performance/confocal-microscopy-attocfm/>
- [9] K. Karrai and R. Warburton, *Superlattices and Microstructures* **33**, 311 (2003).
- [10] A. Högele *et al.*, *Review of Scientific Instruments* **79**, 023709 (2008).
- [11] D. Leonard *et al.*, *Applied Physics Letters* **63**, 3203 (1993).
- [12] H. Drexler *et al.*, *Physical Review Letters* **73**, 2252 (1994).
- [13] R. Warburton *et al.*, *Nature* **405**, 926 (2000).
- [14] R. Warburton *et al.*, *Physical Review B* **11**, 113303 (2002).
- [15] A. Högele *et al.*, *Phys. Rev. Lett.* **93**, 217401 (2004).
- [16] P. A. Dalgarno *et al.*, *Physical Review B* **77**, 245311 (2008).
- [17] B. D. Gerardot *et al.*, *Applied Physics Letters* **90**, 221106 (2007).
- [18] F. Wu *et al.*, *Physical Review Letters* **35**, 1426 (1975).
- [19] G. Wrigge *et al.*, *Nature Physics* **4**, 60 (2008).